Available online at www.sciencedirect.com

ScienceDirect

journal homepage: www.elsevier.com/locate/he

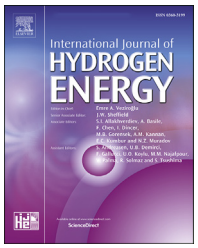

Degradation of methylene blue-ciprofloxacin and hydrogen production simultaneously using combination of electrocoagulation and photocatalytic process with Fe-TiNTAs

Raharjo Muttaqin [a], *Reno Pratiwi* [a], *Ratnawati* [b], *Eniya L. Dewi* [c], *M. Ibadurrohman* [a], *Slamet* [a,*]

[a] *Department of Chemical Engineering, Faculty of Engineering, Universitas Indonesia, Depok, 16424 Indonesia*
[b] *Department of Chemical Engineering, Institut Teknologi Indonesia, Serpong 15314, Indonesia*
[c] *Agency for the Assesment and Application Technology, Puspiptek, Serpong 15314, Indonesia*

HIGHLIGHTS

- Photodegradation of methylene blue and ciprofloxacin is combined with H_2 production.
- Modified Fe-TiNTAs composites enhance the photocatalytic performance.
- The combined process enhances H_2 production more than it does the degradation.

ARTICLE INFO

Article history:
Received 13 January 2022
Received in revised form
30 March 2022
Accepted 4 April 2022
Available online 7 May 2022

Keywords:
Ciprofloxacin
Electrocoagulation
Fe-TiNTAs
Hydrogen
Methylene blue
Photocatalysis

ABSTRACT

The study reported in this paper combines the electrocoagulation and photocatalysis for the simultaneous degradation of methylene blue dyes (MB)-antibiotic ciprofloxacin (CP) and production of hydrogen. The pollutant removal process was conducted by combining adsorption by electrocoagulation and degradation by photocatalysis. Meanwhile, H_2 was produced by reducing the H^+ on the cathode and the photocatalyst surface in a reactor made of acrylic equipped with aluminum as the anode, stainless steel 316 plates as a cathode, Fe-doped titania nanotube arrays (TiNTAs) as a photocatalyst, and a 250-W mercury lamp as the light source. TiNTAs were synthesized via anodization and followed by the successive ionic layer adsorption and reaction (SILAR) method to incorporate Fe as the dopant. In particular, the effects of Fe loading in the composite photocatalyst are investigated. XRD results showed that TiO_2 nanotubes arrays comprise a 100% anatase phase. FESEM, EDX, TEM, and HRTEM analysis confirmed the formation of the nanotubular structure of TiO_2 and the presence of Fe deposited on the surface. The UV–Vis DRS indicated that the bandgap of Fe-TiNTAs reduced with Fe introduction, as compared to that of the undoped TiNTAs. The results showed that accumulation of the produced hydrogen from the combination of electrocoagulation-photocatalytic system is greater than that which is obtained using individual electrocoagulation or photocatalytic system. The combined process exhibited an enhanced degradation ability of methylene blue and ciprofloxacin, as well as in the H_2 production.

* *Corresponding author.*
E-mail address: slamet@che.ui.ac.id (Slamet).
https://doi.org/10.1016/j.ijhydene.2022.04.031
0360-3199/

Introduction

One of the environmental issues that have not been fully resolved is indiscriminate disposal of hospital wastewater which contains dyes and antibiotics that can disrupt the balance of the aquatic ecosystem. Ciprofloxacin ($C_{17}H_{18}FN_3O_3$) is an example of antibiotics that is commonly used to treat respiratory tract infections, gastrointestinal infections, and urinary tract infections caused by bacteria [1], and it is widely detected in the environment with concentrations from 5.6 $\mu g\,L^{-1}$ to 10 $\mu g\,L^{-1}$ [2]. Meanwhile, methylene blue ($C_{16}H_{18}ClN_3S$) is also widely used in hospitals for diagnosis, surgery, and methemoglobinemia [3]. The accumulation of these two toxic elements in public waters may severely impact living things.

Electrocoagulation is one of the technologies widely used in hospital wastewater treatment due to its ability to effectively remove dissolved pollutants in high concentrations. This technology is an electrochemical method that uses direct current to reduce turbidity and color, thereby leading to the *in situ* formation of coagulant by aluminum or iron electrodes [4]. Metal ions at the anode react with hydroxides (OH^-) to produce coagulant, while the reduction of water at the cathode produces OH^- and hydrogen ions (H^+) which will further be transformed to H_2. The latter product is important because, with industrial development, the production of renewable energy such as H_2 is also needed to replace the fossil energy that depletes over time. This thereby gives an idea of integrating a system that effectively eliminates pollutant, while at the same time offers production of H_2 as a source for green energy. The presence of hydrogen (H_2) also helps to float flocculated particles on the surface of the wastewater [5]. However, based on the mechanism, the ability of electrocoagulation is limited to removing and degrading dissolved pollutants. Therefore, further processing is needed to handle the formed coagulant and prevent it from polluting the environment. One promising strategy to circumvent this issue is by employing photocatalysis that is capable of chemically degrading pollutants and, at the same time, generating hydrogen. The utilization of photocatalysis for simultaneous pollutant degradation and hydrogen production has been addressed by many authors [6–8] due to its reliability and cost-effectiveness.

Some researchers have conducted studies on ways to improve the effectiveness of wastewater treatment by combining the two technologies, namely electrocoagulation and photocatalysis. In the direct order (i.e. electrocoagulation followed by photocatalysis), the sequential combination of these techniques has increased the solute removal efficiency by more than 90% [9–12]. Meanwhile, in the reverse order (i.e. photocatalysis followed by electrocoagulation), this process also enhances its efficiency [11,12].

In our previous study, we developed a method capable of treating wastewater using electrocoagulation and photocatalysis in one reactor simultaneously. The optimal conditions, which include the electrical voltage used in electrocoagulation, pH, photocatalyst morphology, and photocatalyst dopants, had been studied to obtain a functioning system that is capable of removing dissolved pollutants [5,13,14]. Since electrocoagulation and photocatalytic technologies produce hydrogen during the water purification process (pollutants removal), therefore, efforts to increase H_2 production are also conducted through the modifications.

Semiconducting TiO_2 is used as the photocatalyst in this combined system due to its abundance, cost-effectiveness, photoactivity, and excellent stability [9]. Along with these virtues, some drawbacks of TiO_2 have also been acknowledged, namely low surface area and relatively high bandgap (3–3.2 eV), which constitutes that it can only be activated by illumination of the ultraviolet light. Another obstacle in using TiO_2 is its high recombination rate between the holes and the excited electrons, thereby preventing the occurrence of the oxidation-reduction reaction on the surface [9,14]. These intrinsic conditions affect the effectiveness of TiO_2 as a photocatalyst in its application. Therefore, the non-metal and noble metal doping and TiO_2 sensitization with e.g. CdTe, Bi_2WO_6, Bi_2MoO_6 have been used to eliminate the drawbacks [6,15,16]. Introducing the transition metal ions as dopant can give rise to the formation of a doping energy level between valence and conduction bands of TiO_2. Furthermore, this dopant may act as electron-holes trapping, which enhances the photocatalytic performance of TiO_2.

As mentioned above, a combination of electrocoagulation and photocatalytic processes in waste treatment and hydrogen production has been developed in our previous studies. For example, we used TiO_2 nanoparticles coated with aluminum to expand the photocatalyst surface, thereby increasing its ability to degrade dye pollutants in the simultaneous processes [5]. We furthermore developed the combined processes using TiO_2 nanotube Arrays (TiNTAs), which has a wider specific surface area with excellent response to photon energy exposure and better electron transport. Therefore, the photocatalytic process becomes more effective in degrading dissolved pollutants [13]. Subsequently, we improved the performance of TiNTAs by depositing CuO as an electron trapper and providing a smaller energy band gap of the photocatalyst [14]. The modifications managed to suppress the recombination rate of electron-hole pairs and be more responsive to visible light exposure.

Doping with transition metal ions such as Pt, Pd, Ag, Fe on TiO_2 increases photocatalytic activity in visible light exposure (reduce the band-gap), and trap electrons to reduce electron-hole recombination [14]. Fe is one of the transition metals capable of increasing photoactivity by inhibiting electron-hole recombination and effectively increasing hydrogen production [17,18]. Furthermore, Fe is abundant, cost-effective, and of particular interest due to its ability to degrade organic and inorganic pollutants. Fe^{+3} can also be easily integrated into the TiO_2 lattice because its radius (0.64 Å) is close to that of Ti^{+4} (0.68 Å) [18,19]. Accordingly, in this paper we report the combination of electrocoagulation and photocatalytic process in a novel, integrated system (single reactor) using Fe-TiNTAs for simultaneous degradation of methylene blue-ciprofloxacin and hydrogen production. The pollutant model used, which is a mixture of methylene blue-ciprofloxacin contained in hospital waste, has also not been widely studied.

This study analyzed the combination process of electrocoagulation and photocatalysis using Fe-TiNTAs to degrade a mixture of ciprofloxacin and methylene blue as a wastewater model and to produce hydrogen simultaneously. Fe was

introduced on TiNTAs using the successive ionic layer adsorption reaction (SILAR) method, and the amount of Fe deposited on TiO_2 was varied. The photocatalyst characterizations were conducted using FESEM, EDX, TEM, XPS, XRD, and UV–Vis DRS, and the results were used to examine the effect of specific parameters on ciprofloxacin-methylene blue removal and hydrogen production. Finally, this study aims to obtain an effective, environmentally friendly, and relatively inexpensive system for degrading dissolved pollutants to produce hydrogen.

Experimental

Preparation TiNTAs and synthesis of Fe-TiNTAs

A titanium plate (Shaanxi Yunzhong Metal Technology Co., LTD) of 8 cm × 4 cm was mechanically polished with sandpaper and mixed in a chemical solution of HF (Merck), HNO_3 (Merck, 65%), and distilled water by volume ratio of 1:3:46 for 1 min. The titanium plate was then rinsed with distilled water and sonicated for 20 min to remove all impurities completely. Anodization was carried out to obtain the TiNTAs photocatalyst using a glycerol electrolyte solution containing 0.5% wt NH_4F and 25%v/v volume of water. A platinum plate of 8 cm × 4 cm and titanium were used as the cathode and the anode, at a voltage of 50 V for 2 h.

Deposition of Fe on TiNTAs was carried out using successive ionic layer adsorption and reaction (SILAR) method with $Fe(NO_3)_3.9H_2O$ (Merk analytical, EMSURE® ACS) as the a precursor for Fe. TiNTAs plates were immersed in $Fe(NO_3)_3$ solution at various concentrations of 0.05 M, 0.07 M, 0.1 M, and 0.2 M, and rinsed in distilled water for 30 s. The samples were then dried at room temperature for 30 s. The procedure counts as one SILAR cycle, and it was repeated 20 times to ensure sufficient Fe deposition. The Fe deposited on TiNTAs was then calcined in a furnace at 500 °C for 3 h to improve their crystallinity.

Characterizations of Fe-TiNTAs

The morphology and superstructure of the prepared samples (TiNTAs and Fe-TiNTAs) were scrutinized using Field Emission Scanning Electron Microscope (FESEM, FEI Inspect F50, and JEOL JIB-4610F) and Transmission Electron Microscope (TEM, FEI Tecnai G2 20 S-Twin). X-ray photoelectron spectroscopy (XPS, ULVAC-HPI Quantera II) was performed to evaluate the oxidation states of Ti, O and Fe, which are estimated from element peak areas of XPS signals. X-ray diffraction analysis (XRD, Shimadzu 7000 Maxima-X) was employed to determine the crystal structure and material composition at a voltage of 40 kV and a current of 30 mA using Cu–Ni α radiation ($\lambda = 0.15406$ nm) as the beam source. The crystallite size of the specimen was estimated from the full-width half-maximum (FWHM) of XRD peaks using the Scherrer equation [20]. Band-gap energy values were obtained using the UV–visible diffuse reflection spectra (Harrick Scientific, Agilent Cary 600 UV–Vis, DRS).

Test on electrocoagulation-photocatalytic system

The performance tests of the electrocoagulation system were carried out in a reactor vessel containing 1-L solution of ciprofloxacin (CP, 10 ppm) and methylene blue (MB, 10 ppm) equipped with aluminum (1 mm thick, 10 cm × 4 cm) and stainless steel 316 (1 mm thick, 8 cm × 2.5 cm) plates as the anode and the cathode, respectively. The distance between the two electrodes is 1.5 cm, each one of which is connected to a DC generator (Zhaoxin RXN-605D, 60 V 5 A) set at a voltage of 20 V.

The electrocoagulation-photocatalytic system was tested by combining both technologies in a reactor vessel, as shown in Fig. 1. The same solution conditions were used, and the reactants were stirred throughout the process. The electrocoagulation system used one 316 stainless steel plate (1 mm thick, 8 cm × 2.5 cm) and one aluminum plate (1 mm thick, 10 cm × 4 cm in size) as cathode and anode, respectively. The

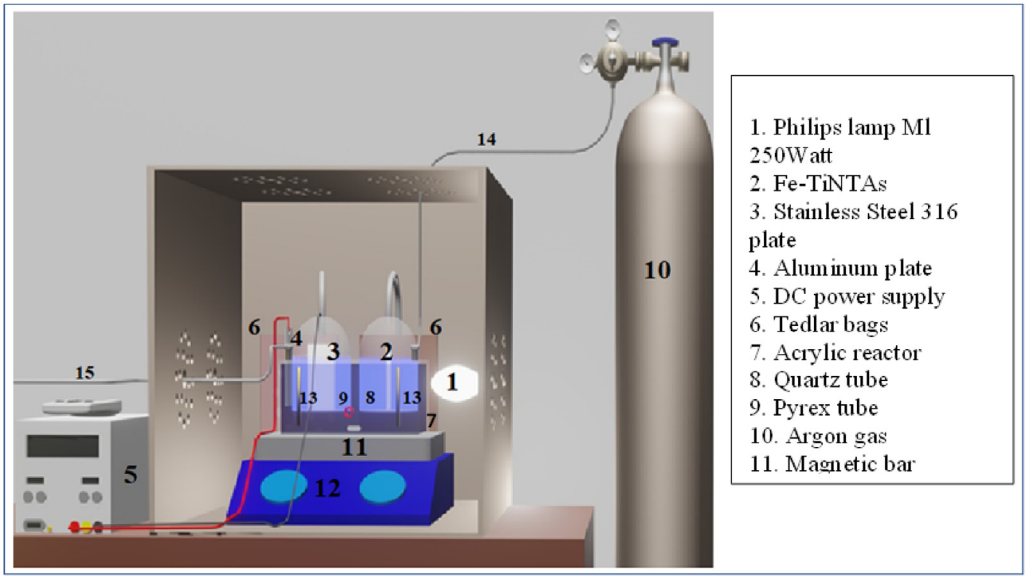

Fig. 1 – Combination of electrocoagulation - photocatalytic reactor system.

8 cm × 4 cm Fe-TiNTAs photocatalyst plate was mounted on the opposite side. The Pyrex tube mounted on the SS-316 plate was connected to a Tedlar bag as a hydrogen collector. During the performance test, and the solution was stirred continuously, while being exposed to illumination from a mercury lamp (17.25% UV and 82.75% visible light, 250 W). Prior to each experiment, argon gas flows through the reactor for 5 min to remove oxygen from the system. Measurements were made every hour on changes in the concentration of ciprofloxacin, methylene blue, and hydrogen produced.

Measurement of pollutant removal and hydrogen production

The pollutant samples were separated by centrifugation to remove fine particles from the catalyst capable of affecting the absorption data through a UV–Vis spectrophotometer (Shimadzu, UV Mini 1240). The equipment worked at the wavelength of 665 nm and 336 nm for absorbance measurement of methylene blue and ciprofloxacin, respectively. Equation (1) is used to calculate the decrease in methylene blue and ciprofloxacin concentration as follows:

$$\text{Removal}(\%) = \frac{C_0 - C}{C_0} \times 100\% \quad (1)$$

C_0 and C are the concentration of methylene blue and ciprofloxacin in mg/L (ppm) at initial and at a certain time, respectively. The concentration of hydrogen produced by electrocoagulation and photocatalysis was analyzed every hour using a Gas Chromatography (Shimadzu GC-8A) system equipped with a Molecular Sieve (MS) Hydrogen 5 A column, with a known retention time for argon as the carrier gas.

Results and DISCUSSION

Characterization of modified Fe-TiNTAs

The FESEM characterization was performed to determine the morphology of photocatalyst samples. Based on FESEM results shown in Fig. 2, deposition of Fe does not cause apparent changes on the morphology and nanotubular structure of TiNTAs, which most likely is attributable to small amount of Fe being deposited. Importantly, Fig. 2(b–f) shows that incorporation of Fe into TiNTAs up to 0.2 M does not cause agglomeration and particle clusters that may interfere with the active surface of titania nanotubes. The EDX spectra are shown in Fig. 2 (a), while the average diameter, tube wall, and EDX result of photocatalyst samples are presented in Table 1.

The average diameter and the average wall thickness of the Fe-doped nanotubes decreased with increasing Fe concentration, as informative in Table 1. This is likely because Fe^{3+} possesses a great electron affinity, hence capable of entering the Ti^{4+} crystal lattice. Therefore, the attractive force with O atoms becomes stronger, leading to shrinkage of the nanotube

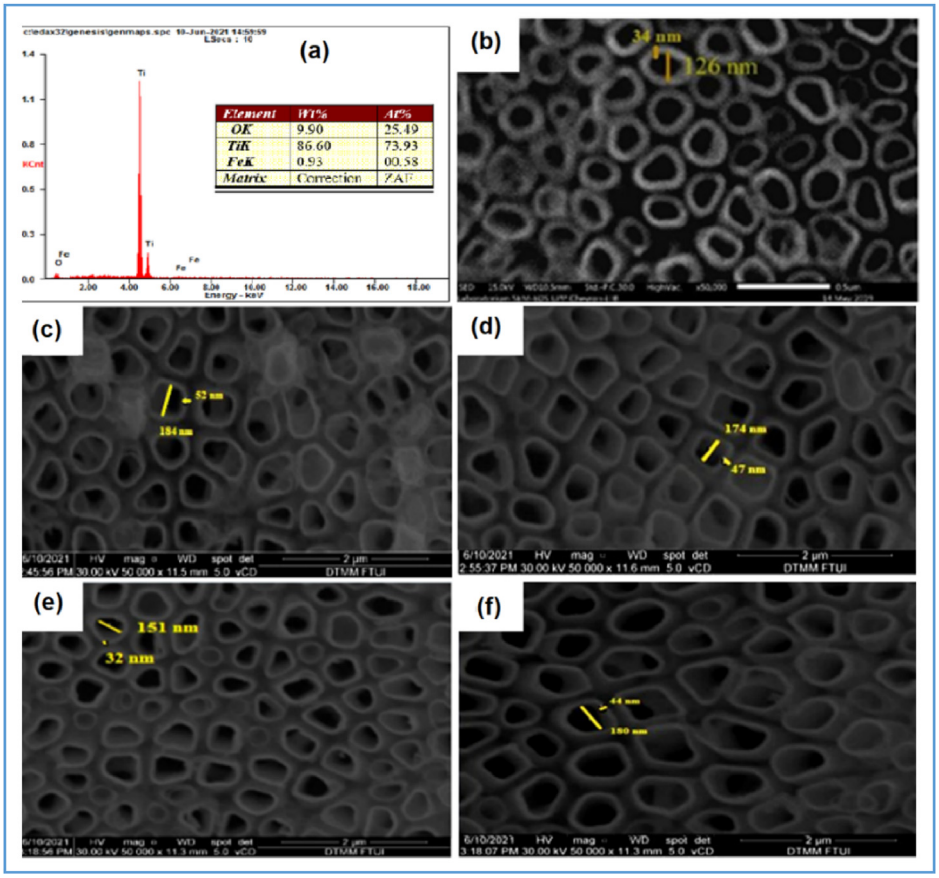

Fig. 2 – (a) EDX spectra of 0.07 M Fe-TiNTAs, FESEM image of (b) TiNTAs, (c) 0.05 M Fe-TiNTAs, (d) 0.07 M Fe-TiNTAs, (e) 0.1 M Fe-TiNTAs, and (f) 0.2 M Fe-TiNTAs at 50,000× magnification.

size. Meanwhile, according to the EDX results, the increase in Fe precursor concentration on TiNTAs is positively correlated, though not proportional, to the eventual loading (wt%) of Fe. Due to the fact that TiO_2 has limited active sites to which Fe particles may attach, the non-linear relationship between Fe loading and the precursor solution is somewhat expected. The trend may thereby be described as a saturation-growth-like model in which the linearity is expected only at low concentrations of Fe precursor, while Fe begins to reach saturation on TiO_2 surface at high concentrations. Importantly, the EDX results (average value from three different areas) confirm that Fe has been deposited on TiNTAs with an expected correlation between the precursor concentration and the eventual loading. TEM analysis was carried out to prove further the presence of Fe deposited on TiNTAs, as shown in Fig. 3.

The TEM and HRTEM micrographs shown in Fig. 3 further clarify the presence of Fe that are evenly distributed on the TiNTAs surface. Fig. 3(a) illustrates that Fe is well dispersed along the surface of TiNTAs, not only on the tube mouth but also on the tube wall. Based on Fig. 3(b), the presence of the anatase crystal phase (101) with the corresponding d-spacing value of 0.359 nm is confirmed. On the other hand, the crystal phase (002) with lattice fringes of 0.687 nm confirms the presence of Fe_2O_3. This result is in good agreement with previous reports [21]. Fig. 3(a) presents the morphology of the nanotubes, revealing a diameter of ca. 150 nm. This further corroborates our findings from the FESEM data presented in Table 1. Fig. 3(a) also shows that the nanotube is larger on the bottom part than it is on the upper part. Such a profile is likely to affect the absorption of photons, as well as access for Fe dopant to the interior of the tubes.

The valence states and chemical compositions of the photocatalyst samples were studied by XPS. Four elements were detected in the survey spectrum, namely Fe, Ti, O, and C as shown in Fig. 4(a). Fig. 4(b) infers the observation of peak signals of Fe at 710.92 eV and 724.02eV, attributable to Fe $2p_{3/2}$ and Fe $2p_{1/2}$ respectively [22]. The results are indicative of the presence of Fe in the Fe-TiNTAs composite. Meanwhile, in Fig. 4(c), the XPS spectra of Ti 2p at a binding energy of 458.33 eV and 464.03 eV are assigned to Ti $2p_{3/2}$ and Ti $2p_{1/2}$ respectively, which indicates the presence of Ti element in the state of Ti^{4+} on the photocatalyst sample [6]. As depicted in Fig. 1(a), the XPS signal of O 1s is observable at the binding energy of 530.5 eV, corresponding to O in the lattice structure of TiO_2 [6]. Furthermore, the C 1s peak at the binding energy around 284 eV may indicate external carbon contamination [7].

The X-Ray Diffraction (XRD) characterization was conducted to obtain information on the structure and crystallite phases of the nanocomposites. Fig. 5 shows the XRD pattern for TiNTAs compared to 0.2 M Fe-TiNTAs. The observed peaks at 2θ of 25.3°, 37.7°, 48.4°, and 54° correspond to the diffraction peaks in the fields of (101), (004), (200), and (105), which conform to an anatase phase according to the JCPDS card No. 21-1272 [18]. Peaks at 2θ values of 27.4° and 36°, which correspond to the rutile crystal phase, were not observed, indicating that all synthesized TiNTAs and Fe-TiNTAs photocatalysts are composed of 100% anatase crystal.

For the Fe-TiNTAs sample, no signal is observed in the XRD patterns for iron-based oxides, while the absence of an impurity phase or a new diffraction peak for the 0.2 M Fe-TNTAs may be because the characterization technique used is not very sensitive to the low content of Fe^{3+}. This may also be

Table 1 – EDX analysis results of the synthesized nanocomposites.

Photocatalyst	Average tube diameter (nm)	Average tube wall thickness (nm)	wt% of Element		
			Fe	Ti	O
TiNTAs	126	34	0	81.15	18.74
0.05 M Fe-TiNTAs	184	52	0.47	86.60	12.92
0.07 M Fe-TiNTAs	174	47	0.93	89.15	9.90
0.1 M Fe-TiNTAs	151	32	1.09	88.33	10.57
0.2 M Fe-TiNTAs	180	44	1.30	88.05	10.63

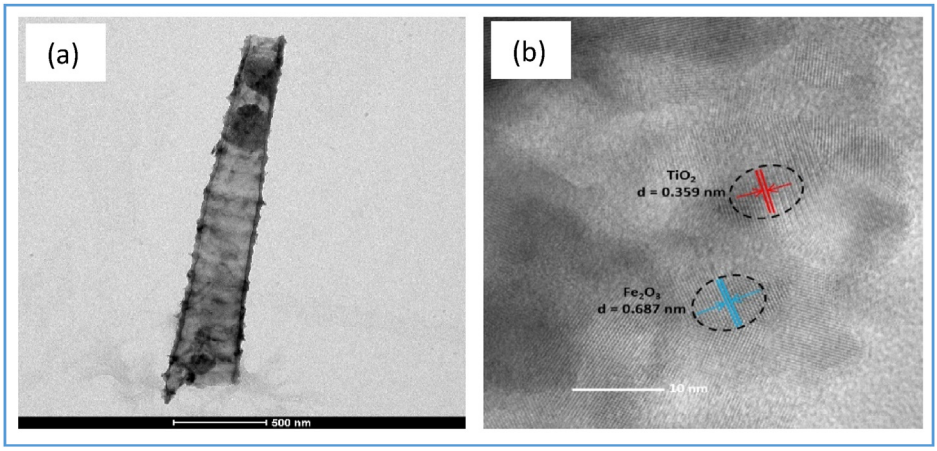

Fig. 3 – (a) TEM and (b) HRTEM image for Fe-TiNTAs.

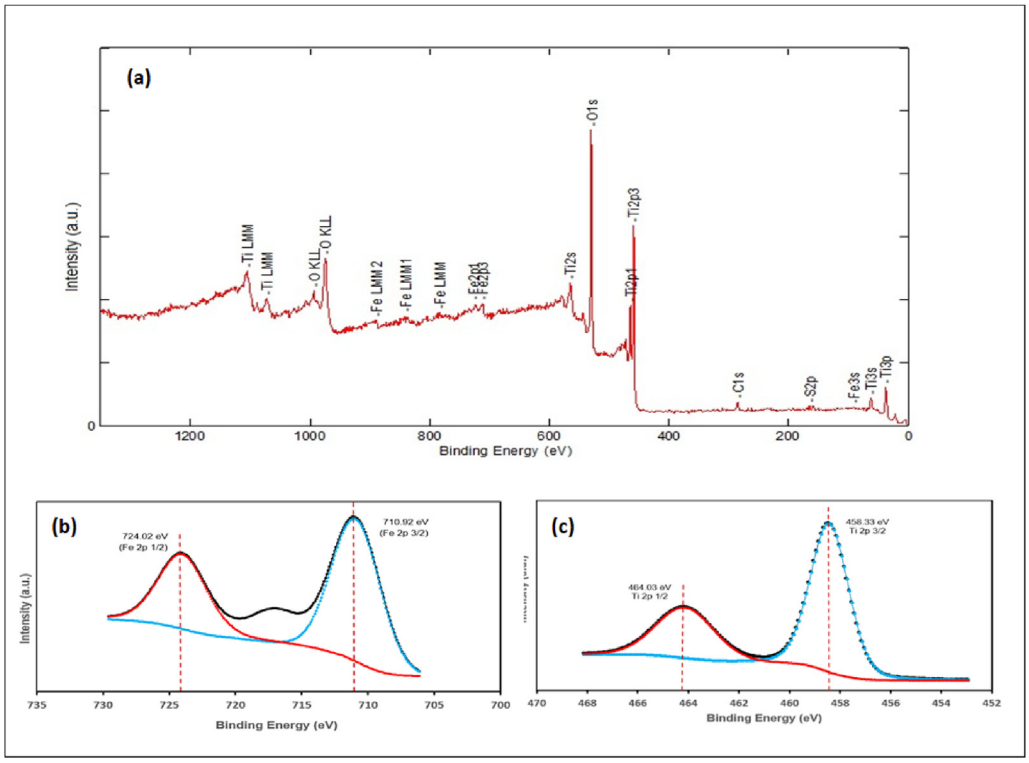

Fig. 4 – Survey spectra of (a) 0.1 M Fe-TiNTAs, and high resolution XPS spectra of (b)Fe 2p, and (c) Ti 2p.

attributed to the Fe^{3+} substituting Ti^{4+} in the TiO_2 lattice structure. The low concentration of Fe deposited onto the TiO_2 nanotubes (which agrees with the EDX results) was advantageous in this case as they did not lead to a shading effect, hence the active site of the TiO_2 nanotube photocatalyst is not reduced. The presence of Fe in 0.2 M Fe-TiNTAs increases the crystallite size from 19 to 20 nm for the TiNTAs and Fe-TiNTAs respectively. This condition is related to the presence of a sintering effect at high temperatures, which can increase the catalyst's crystal size. Another possibility that causes the increase in crystal size is the presence of Fe dopant, which has a higher conductivity of 79.5 W/mK, compared to the pure TiO_2 of only 4.8 W/mK.

The UV–Vis DRS analysis results shown in Fig. 6 are used to evaluate the bandgap, employing the Kubelka–Munk equation when $[F(R).hv]^{0.5} = 0$ by extrapolating the linear region of the $(F(R)\ hv)^{0.5}$ curve vs energy (hv) [23]. The bandgap of Fe-TiNTAs with 0.05 M, 0.07 M, 0.1 M and 0.2 M dopant solutions were 3 eV, 2.94 eV, 2.9 eV and 2.78 eV respectively, and less than that of pure TiO_2 nanotubes (3.16 eV). The band-gap energy decreased due to the presence of Fe dopant in TiO_2 nanotubes. The reduced bandgap leads to extended absorption of light into the visible-light region, as the absorption onset is red-shifted to longer wavelength range.

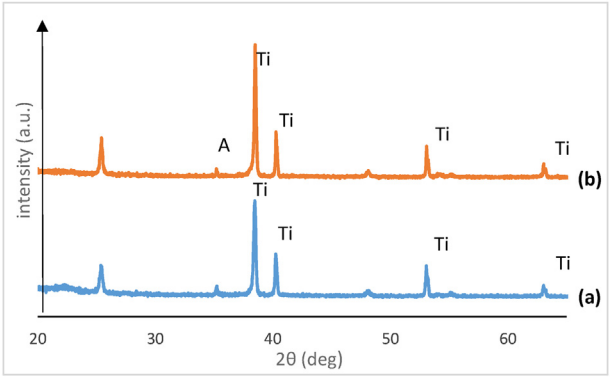

Fig. 5 – XRD patterns of (a) TiNTAs and (b) Fe-TiNTAs.

Electrocoagulation test on pollutant removal and H_2 production

Electrocoagulation is a process that uses electrochemical principles to oxidize aluminum (Al) or Fe metal on the anode plate, which reacts with hydroxyl ions in solution to form a coagulant. This study used oxidized anode aluminum (Al) to form Al^{3+} ions on the surface of the anode plate, as shown in Equation (2). Al^{3+} ions dissolve in the solution, which is then bound to hydroxyl ions to form a coagulant $Al(OH)_3$ and finally adsorb the pollutants according to Equations (4) and (5). Meanwhile, at the cathode, electrons reduce H_2O and produce hydrogen (Equation (3)) as follows [24]:

$$\text{Anode: } Al(s) \rightarrow Al^{3+}(aq) + 3e^- \quad (2)$$

$$\text{Cathode: } 2H_2O(aq) + 2e^- \rightarrow 2OH^-(aq) + H_2(g) \quad (3)$$

$$Al_3 + (aq) + 3H_2O\ (aq) \rightarrow Al(OH)_3\ (s) + 3H + (aq) \quad (4)$$

$$Al(OH)_3(s) + \text{Pollutant} \rightarrow \text{Pollutant} - Al(OH)_3\ (s) \quad (5)$$

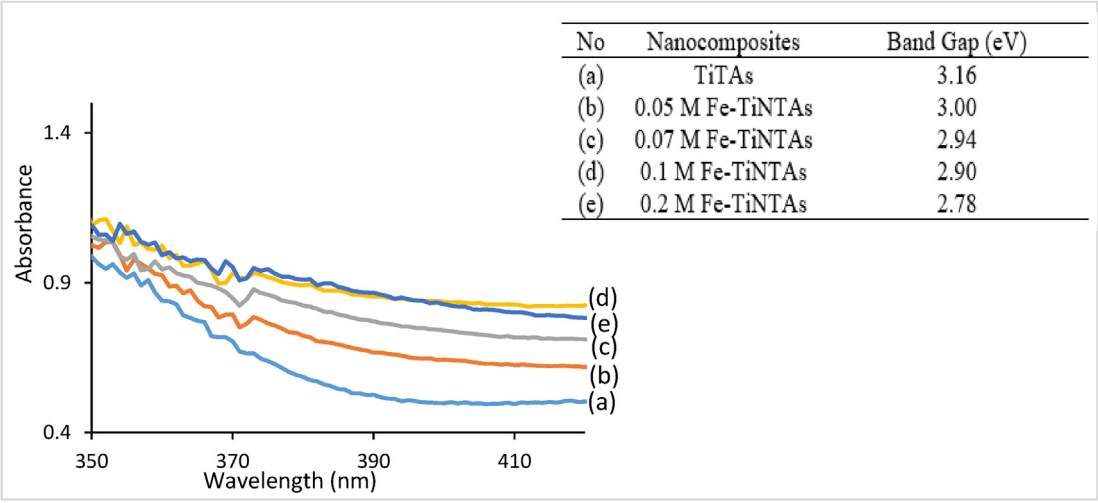

No	Nanocomposites	Band Gap (eV)
(a)	TiTAs	3.16
(b)	0.05 M Fe-TiNTAs	3.00
(c)	0.07 M Fe-TiNTAs	2.94
(d)	0.1 M Fe-TiNTAs	2.90
(e)	0.2 M Fe-TiNTAs	2.78

Fig. 6 – UV–Vis DRS spectrum of (a) TiNTAs, (b) 0.05 M Fe-TiNTAs, (c) 0.07 M Fe- TiNTAs, (d) 0.1 M Fe- TiNTAs and (e) 0.2 M Fe- TiNTAs.

The electrocoagulation process at an electrical voltage of 20 V is employed to remove dissolved CP and MB pollutants in the solution, based on the optimum results in the previous study [14]. Although the voltage value is linearly correlated with the amount of coagulant produced, a value greater than the optimum condition insignificantly affects the process [25]. The initial pH of the solution plays an essential role in the effectiveness of the electrocoagulation process [26]. Furthermore, an initial pH of 10 was used to obtain alkaline conditions that were not too concentrated and capable of working adequately in producing coagulant at aluminum electrodes in slightly alkaline conditions [25]. The process was conducted for 4 h, based on the optimal reaction time in the previous study [14].

Fig. 7 shows the process of removing dissolved pollutants (a mixture of CP and MB) and the cumulative amount of hydrogen produced using the electrocoagulation process. The result shows that the system managed to remove MB than CP rather effectively. It is understandable because the presence of hydroxyl groups causes the surface of the coagulant to be negatively charged and is responsible for its ability to adsorb dissolved pollutants [27]. The MB is easily attracted to the negative charges of the surface of the coagulant because it is a cationic dye. On the other hand, CP is a chemical whose charge and solubility depend on the pH of the solution. During the process with initial pH of 10, the solution pH increases due to the continuous generation of hydroxyl ions (OH^-) in the cathode, while CP is negatively charged [9,28]. Under these conditions, the ability of the negatively charged coagulant becomes weaker in facilitating the binding process.

During the electrocoagulation process, the cathode produces gas bubbles, which carries the impurities in the water surface. In this case, the voltage and the reaction time significantly affect the effectiveness of simultaneous pollutant removal and H_2 generation. The voltage on the electrocoagulation system affects the hydrogen produced on the cathode surface. The greater the applied voltage, the more Al^{3+} ions are released at the anode. The ions than interact with OH^- and, due to alkaline conditions, the reaction equilibrium shifts to the direction of the products, generating more electrons. As electrons are generated, the production of H_2 effectively takes place at the cathode, thereby bringing the pollutants to the surface for the floc to be easily concentrated,

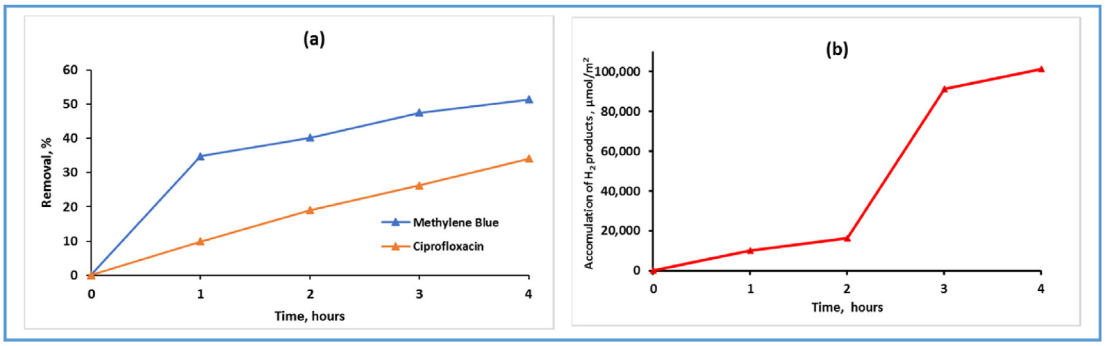

Fig. 7 – Electrocoagulation process at 20 V with the initial pH of 10 for (a) removal of methylene blue and ciprofloxacin, (b) hydrogen production. (For interpretation of the references to color in this figure legend, the reader is referred to the Web version of this article.)

collected, and separated. A low voltage was chosen to allow less coagulant effects because floating coagulants are carried away by the hydrogen formed during the reaction. Fig. 7(b) shows the time course of the hydrogen evolution, in which it is evident that *ca.* 100 μmol/m^2 of hydrogen is generated after 4 h reaction. It is worth noting that the abrupt increase in hydrogen production between 2 h and 3 h is likely due to the saturation of hydrogen in the solution before it bubbles out from the solution. The rate becomes slower afterward as the product concentration becomes higher in the solution.

Photocatalysis test on pollutant removal and H_2 production

The presence of Fe dopant at TiNTAs photocatalysts, as proven in the FESEM/EDX and TEM/HRTEM characterization, plays a significant role in photocatalyst performance, as it enhances the degradation of methylene blue and ciprofloxacin. The higher the concentration of Fe deposited in TiNTAs, the more effective the degradation of pollutants and hydrogen production. Fig. 8 shows a significant increase in the performance of Fe-TiNTAs as compared to the pure TiNTAs photocatalyst, even with the lowest dopant concentration (0.05 M Fe). According to crystal field theory, Fe^{2+} and Fe^{4+} are relatively unstable compared to Fe^{3+}. These reactions favor the formation of hydroxyl radicals or superoxide, as follows:

$$Fe^{3+} + e^-_{cb} \rightarrow Fe^{2+} \quad (electron\ trapper) \tag{6}$$

$$Fe^{2+} + O_2 \rightarrow Fe^{3+} + O_2^- \quad (migration) \tag{7}$$

$$Fe^{3+} + h^+_{vb} \rightarrow Fe^{4+} \quad (hole\ trapper) \tag{8}$$

$$Fe^{4+} + OH^- \rightarrow Fe^{3+} + \bullet OH \quad (migration) \tag{9}$$

Fig. 8(a) and (b) show the effects of the Fe concentration deposited in TiNTAs. The greater the amount of Fe deposited, the smaller the energy band-gap, thereby facilitating pollutant degradation and hydrogen production. However, the addition of Fe at a concentration of 0.2 M with an energy band-gap of 2.78 eV, this photocatalyst has reduced in the photocatalytic activity.

In this experiment, the optimum condition was achieved when the Fe concentration added to TiNTAs was 0.1 M. Similar results were also found in the previous research [17,22], indicating that the higher the concentration of optimum condition, the lower the photocatalyst activity obtained. This is because, at a higher concentration of Fe deposited on TiNTAs, Fe acts as a recombination center for electron-holes pairs before diffusing into the TiO_2 crystal lattice with the ability to agglomerate on the surface to form the Fe_2O_3 phase [29]. Fe^{3+} ions can also act as a recombination center causing deterioration of reducing photocatalytic activity [19] according to the following reactions:

$$Fe^{2+} + h^+_{vb} \rightarrow Fe^{3+} \ (recombination) \tag{10}$$

$$Fe^{4+} + e^-_{cb} \rightarrow Fe^{3+} (recombination) \tag{11}$$

$$Fe^{4+} + Fe^{2+} \rightarrow 2Fe^{3+} (recombination) \tag{12}$$

$$Fe^{4+} + Ti^{3+} \rightarrow Fe^{3+} + Ti^{4+} (recombination) \tag{13}$$

According to Fig. 8 (c), the MB removal is better than that of CP. As shown in Fig. 9, the Fe-TiNTsA photocatalyst is more easily activated on visible light illumination and generates hydroxyl radicals when used in an aqueous solution. Under preferable conditions, more hydroxyl ions are oxidized by the holes on the Fe-TiNTAs photocatalyst to become hydroxyl radicals (•OH) capable of degrading pollutants. The positively charged methylene blue becomes more easily adsorbed on the negatively charged catalyst surface in an alkaline condition, which can lead to high degradation efficiency. In contrast, CP,

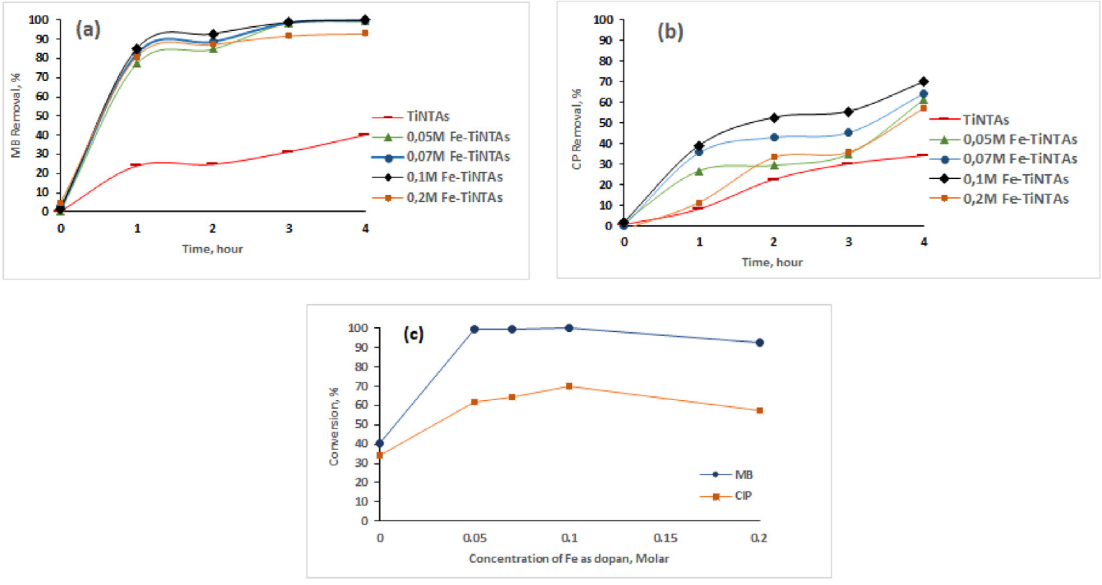

Fig. 8 – Effect of Fe dopant concentration on TiNTAs in the % removal of (a) methylene blue, (b) ciprofloxacin, and (c) methylene blue and ciprofloxacin for 4 h process. (For interpretation of the references to color in this figure legend, the reader is referred to the Web version of this article.)

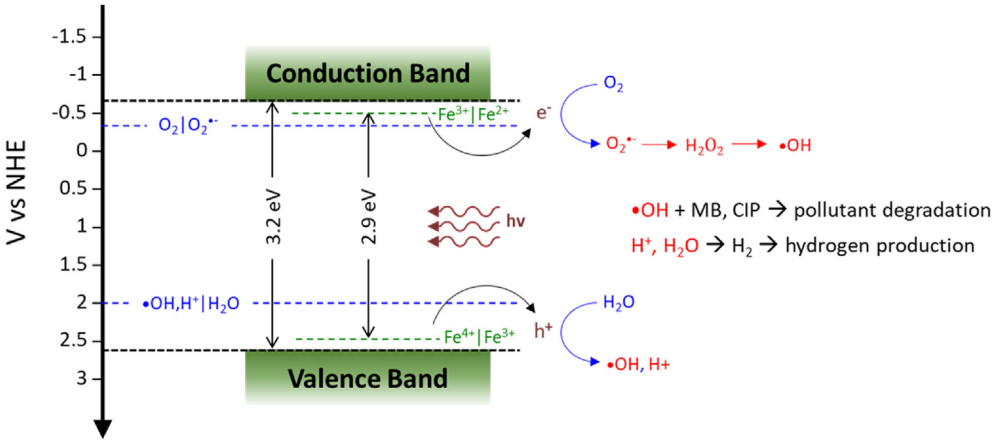

Fig. 9 – Schematic illustration of Fe-TiNTAs photocatalyst in pollutant degradation and hydrogen production.

which has an anionic group in an alkaline environment, reacts with hydroxyl radicals at a slower rate.

In this system, along with photocatalytic degradation of pollutants, hydrogen is also produced. Photon irradiation on TiNTAs causes the excitation of electrons from the valence to the conduction band. The electrons at the surface of the photocatalyst reduce hydrogen ions that are originated from the decomposition water molecules into hydrogen and oxygen as follows:

$$Fe - TiO_2 + h\nu \rightarrow h+ + e^- \quad (14)$$

$$\text{Valence band: } H_2O + 2h+ \rightarrow \frac{1}{2}O_2\,(g) + 2H+ \quad (15)$$

$$\text{Conduction band: } 2H+ + 2e^- \rightarrow H_2(g) \quad (16)$$

In using TiNTAs photocatalyst with various Fe concentrations in the range of 0, 0.05, 0.07, 0.1, and 0.2 M, the hydrogen produced is 16.46, 17.18, 21.71, 27.38 mol, and 14.79 μmol/m^2, respectively, as presented in Fig. 10. The decrease in hydrogen production when Fe content is excessively high suggests the occurrence of recombination centers in the photocatalyst, which decreases the effectiveness of the redox reactions. Then, hydrogen produced is directly proportional to the % decrease in pollutant concentration.

Combination of electrocoagulation and photocatalytic process

Fig. 11 shows the primary set of equipment used in the combination of electrocoagulation and photocatalytic process, where a glass sheath protects stainless steel electrode and Fe-TiNTAs plate to provide more accurate measurements of hydrogen. The combined processes of electrocoagulation and photocatalysis is superior to the individual process, as presented in Fig. 12. In the case of combined processes, two

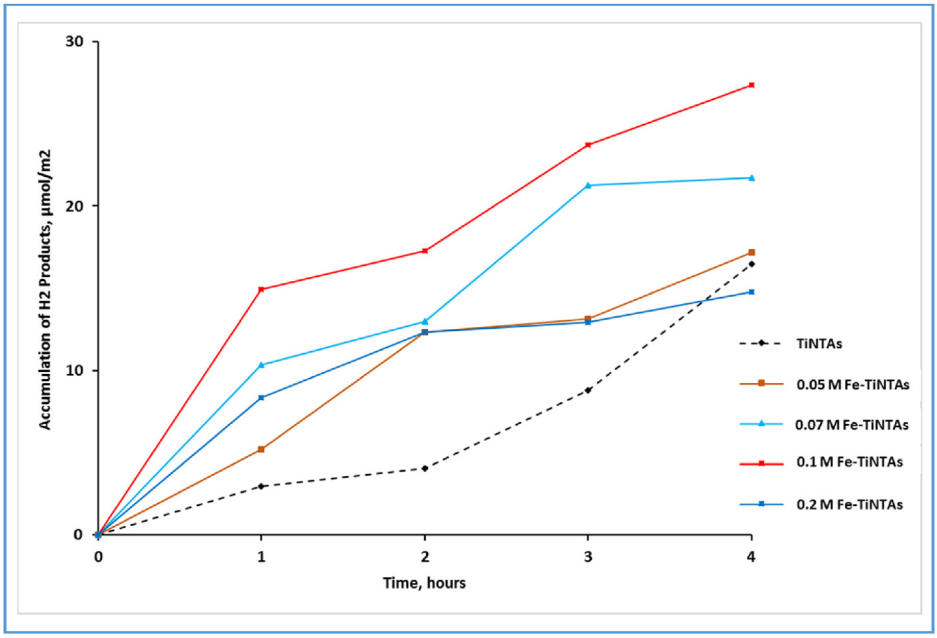

Fig. 10 – Accumulation of the H_2 generated on the photocatalytic process with a variation of Fe deposited on TiNTAs with the initial pH 10.

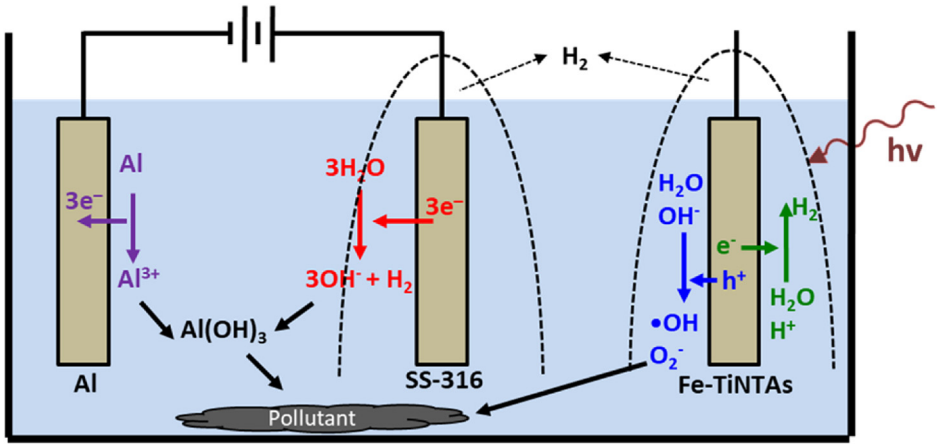

Fig. 11 – Illustration of the combination electrocoagulation and photocatalysis.

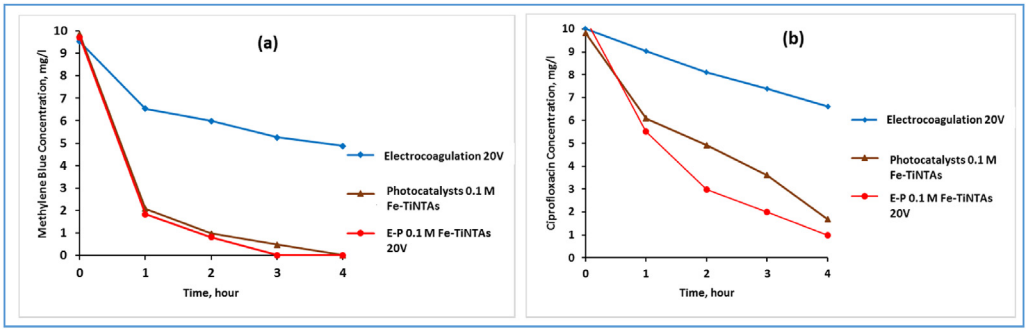

Fig. 12 – Degradation of (a) methylene blue and (b) ciprofloxacin as a function of various processes. (For interpretation of the references to color in this figure legend, the reader is referred to the Web version of this article.)

mechanisms simultaneously drive the process as a whole, namely pollutant removal via adsorption by the coagulant $Al(OH)_3$ in the electrocoagulation process and the oxidation reaction of pollutants by •OH or $•O^{2-}$ radicals generated from the photocatalytic process.

However, despite having the same trend, where the degradation ability of the simultaneous electrocoagulation-photocatalysis (E-P) process is better than the individual, there are differences in the performance of each pollutant. Fig. 12(a) and (b) show that methylene blue is easier to remove than ciprofloxacin, as elucidated in the previous section. It also indicates that the type of pollutant affects the effectiveness of pollutant removal through the concurrent processes. In removing methylene blue and ciprofloxacin, the photocatalytic process is dominant as compared to electrocoagulation. It means that the pollutants react more easily with the hydroxyl radicals generated in an alkaline solution. From this study, the simultaneous use of the E-P process does not provide significant changes. As for the results in Fig. 12(b), it shows that, after 2 h, the difference in ciprofloxacin degradation between the use of photocatalyst only and that of combination with electrocoagulation is noticeable. After 2 h of illumination, the combined process managed to degrade 70% ciprofloxacin, while only 50% is achieved when only photocatalyst is present. At the third hour, ciprofloxacin is degraded by 80% in the case of the combined processes, and only 63% in the case of photocatalysis. Finally, after 4 h, the combined processes managed to reach 90% decomposition of ciprofloxacin, while photocatalysis can only impose 83% of decomposition.

Fig. 13 shows that hydrogen production using the combined electrocoagulation and photocatalytic processes increases H_2 production by 98.74% as compared to the total H_2 produced by electrocoagulation and photocatalysis systems. In the electrocoagulation process using aluminum electrodes, Al^{3+} ions are formed, which react with OH- from the solution to form a coagulant. The continuous process causes the concentration of OH- in the solution to decrease. In the principle of equilibrium, a solution containing water as the solvent medium reduces the OH- in an excess concentration of H^+ ions in the solution, thereby leading to the production of hydrogen [26]. The use of electrocoagulation and photocatalysis processes simultaneously will consume OH- more intensively due to the formation of coagulants in the electrocoagulation section and the oxidation reaction of the formation of hydroxyl radicals in the photocatalysis, thereby leading to excessive concentration of H^+ in the solution.

The type of pollutants (single or mixture) affect the performance of the degradation process, as shown in Fig. 14 (a) and (b). It is better to use a mixture of the two pollutants than individual MB or CIP in the solution because it forms a concentrated solution that facilitates degradation reaction in

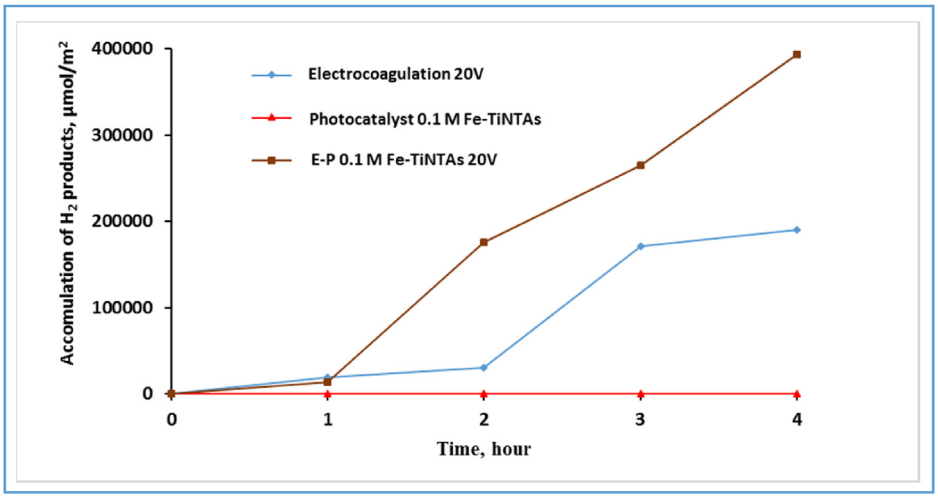

Fig. 13 – Hydrogen production as a function of various process.

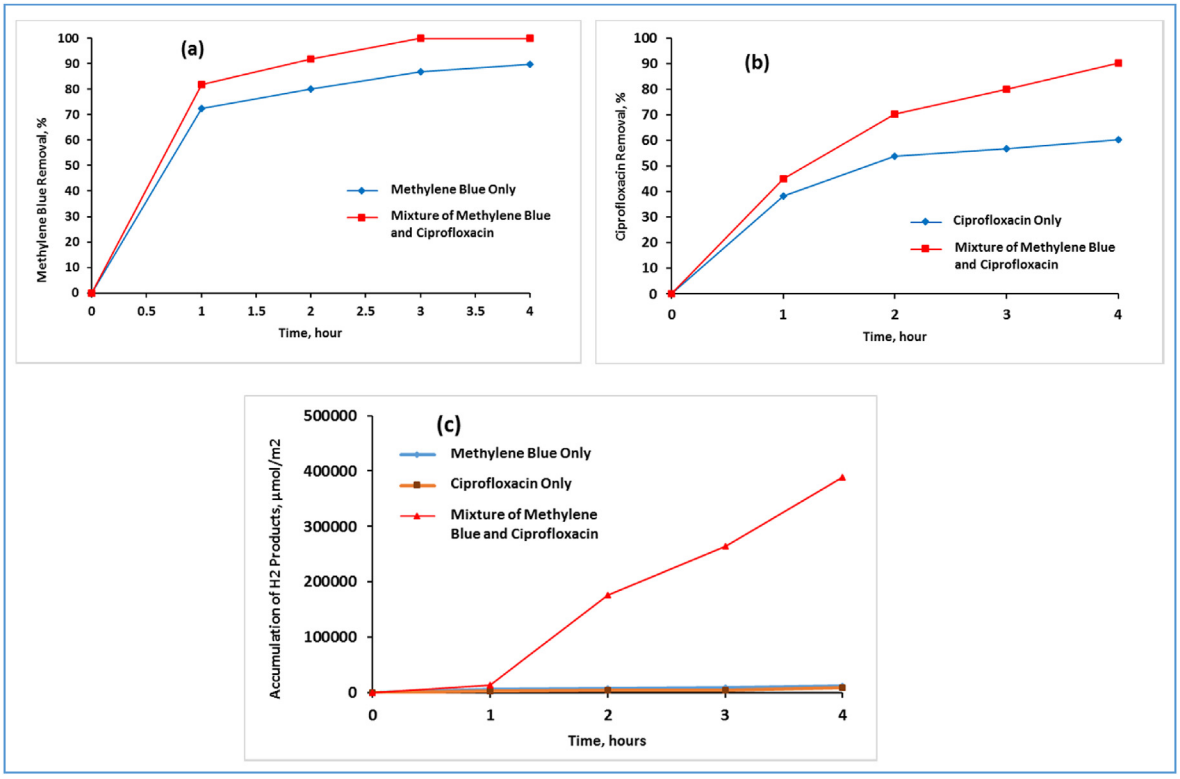

Fig. 14 – Degradation of (a) methylene blue (b) ciprofloxacin and, (c) H_2 production at various pollutants (single and mixture) with combination process of electrocoagulation and photocatalytic process. (For interpretation of the references to color in this figure legend, the reader is referred to the Web version of this article.)

photocatalysis. Moreover, the adsorption process in electrocoagulation runs more effectively and therefore increases the ability to remove dissolved pollutants and produce hydrogen. The more intensive the process of removing pollutants from the solution, the greater the consumption of OH- solution. This then leads to abundant H^+ ions in the solution. Consequently, the possibility of H^+ ions undergoing a reduction reaction to produce hydrogen gas is more significant, as shown in Fig. 14(c).

Conclusion

In conclusion, this study analyzed the simultaneous treatment of mixed waste containing methylene blue dye and ciprofloxacin. Fe-TiNTAs have been effectively fabricated by an anodization and a SILAR method. The FESEM results confirm the formation of the nanotubular structure as it is also supported by TEM images. The EDX spectra of Fe-TiNTAs

indicated that Fe was deposited on titania nanotubes with optimum conditions for the degradation of pollutants using the photocatalytic system with a precursor solution concentration of 0.1 M Fe. The effect of Fe dopant in TiNTAs reduces the band-gap from 3.16 eV to 2.90 eV for the optimum concentration of 0.1 M Fe. Meanwhile, the absorbance spectra of Fe-TiNTAs shifted to the visible light domain, which verified that the presence of Fe induced more optimal light absorption in the visible region. However, increasing the concentration of Fe to 0.2 M resulted in lower photocatalytic activity, most likely due to the fact that excessive doping promotes recombination, although the band gap is further reduced. The degradation of mixed waste containing methylene blue and ciprofloxacin with a combination of electrocoagulation and photocatalysis with Fe-TiNTAs has also been evaluated. The combination of the electrocoagulation and photocatalytic processes managed to generate 393 $\times$ 10^3 $\mu mol/m^2$, as compared to the electrocoagulation and photocatalytic methods with 190 $\times$ 10^3 and 27 $\mu mol/m^2$, respectively. On the other hand, the combined electrocoagulation and photocatalysis system exhibited an enhanced degradation ability for methylene blue and ciprofloxacin as well as the production of H_2.

Declaration of competing interest

The authors declare that they have no known competing financial interests or personal relationships that could have appeared to influence the work reported in this paper.

Acknowledgments

This study was financially supported by the program Hibah WCR Dikti 2021 Universitas Indonesia, Contract Number: NKB-386/UN2.RST/HKP.05.00/2021.

REFERENCES

[1] Kraemer SA, Ramachandran A, Perron GG. Antibiotic pollution in the environment: from microbial ecology to public policy. Microorganisms 2019;7(6):180.
[2] Sanseverino I, et al. State of the art on the contribution of water to antimicrobial resistance. Brussels: European Union; 2018.
[3] Lacerda JA, et al. TiO2 decorated sand grains for photodegradation of pollutants: methylene blue and ciprofloxacin study. J Braz Chem Soc 2020;31:201–10.
[4] Ramezanalizadeh H, Manteghi F. Synthesis of a novel MOF/CuWO4 heterostructure for efficient photocatalytic degradation and removal of water pollutants. J Clean Prod 2018;172:2655–66.
[5] Sharfan N, et al. Treatment of batik industry waste with a combination of electrocoagulation and photocatalysis. Chem Eng 2018;9(5).
[6] Zhu S, et al. CdTe and Ag nanoparticles co-modified TiO2 nanotube arrays for the enhanced wastewater treatment and hydrogen production. J Environ Chem Eng 2022:107207.
[7] Jia Y, et al. Construction of Bi2S3-BiOBr nanosheets on TiO2 NTA as the effective photocatalysts: pollutant removal, photoelectric conversion and hydrogen generation. J Colloid Interface Sci 2021;585:459–69.
[8] Cao D, et al. Solvothermal synthesis and enhanced photocatalytic hydrogen production of Bi/Bi2MoO6 co-sensitized TiO2 nanotube arrays. Separ Purif Technol 2020;250:117132.
[9] Boroski M, et al. Combined electrocoagulation and TiO2 photoassisted treatment applied to wastewater effluents from pharmaceutical and cosmetic industries. J Hazard Mater 2009;162(1):448–54.
[10] Santos LM, et al. Dye degradation enhanced by coupling electrochemical process and heterogeneous photocatalysis. J Braz Chem Soc 2015;26(9):1817–23.
[11] Ates H, Dizge N, Yatmaz HC. Combined process of electrocoagulation and photocatalytic degradation for the treatment of olive washing wastewater. Water Sci Technol 2017;75(1):141–54.
[12] Dindaş GB, et al. Treatment of pharmaceutical wastewater by combination of electrocoagulation, electro-fenton and photocatalytic oxidation processes. J Environ Chem Eng 2020;8(3):103777.
[13] Slamet S, Kurniawan R. Degradation of tartrazine and hydrogen production simultaneously with combination of photocatalysis-electrocoagulation. In: AIP conference proceedings. AIP Publishing LLC; 2018.
[14] Pelawi LF, Slamet S, Elysabeth T. Combination of electrocoagulation and photocatalysis for hydrogen production and decolorization of tartrazine dyes using CuO-TiO2 nanotubes photocatalysts. In: AIP conference proceedings. AIP Publishing LLC; 2020.
[15] Wang Q, et al. Morphology regulated Bi2WO6 nanoparticles on TiO2 nanotubes by solvothermal Sb3+ doping as effective photocatalysts for wastewater treatment. Electrochim Acta 2020;330:135167.
[16] Liu Z, et al. Solvothermal fabrication and construction of highly photoelectrocatalytic TiO2 NTs/Bi2MoO6 heterojunction based on titanium mesh. J Colloid Interface Sci 2019;556:92–101.
[17] Dholam R, et al. Hydrogen production by photocatalytic water-splitting using Cr-or Fe-doped TiO2 composite thin films photocatalyst. Int J Hydrogen Energy 2009;34(13):5337–46.
[18] Shi X, et al. A mild in-situ method to construct Fe-doped cauliflower-like rutile TiO2 photocatalysts for degradation of organic dye in wastewater. Catalysts 2019;9(5):426.
[19] Shayegan Z, Haghighat F, Lee C-S. Anatase/brookite biphasic surface fluorinated Fe–TiO2 photocatalysts to enhance photocatalytic removal of VOCs under visible and UV light. J Clean Prod 2021;287:125462.
[20] Muniz FTL, et al. The Scherrer equation and the dynamical theory of X-ray diffraction. Acta Crystallogr A: Found Adv 2016;72(3):385–90.
[21] Finch GI, Sinha K. An electron-diffraction study of the transformation α-Fe2O3 to γ-Fe2O3. Proc Roy Soc Lond Math Phys Sci 1957;241(1224):1–8.
[22] Ismael M. Enhanced photocatalytic hydrogen production and degradation of organic pollutants from Fe (III) doped TiO2 nanoparticles. J Environ Chem Eng 2020;8(2):103676.
[23] Chen Z, Dinh HN, Miller E. Photoelectrochemical water splitting, vol. 344. Springer; 2013.
[24] Mollah MY, et al. Fundamentals, present and future perspectives of electrocoagulation. J Hazard Mater 2004;114(1–3):199–210.

[25] Barrera-Díaz CE, Lugo-Lugo V, Bilyeu B. A review of chemical, electrochemical and biological methods for aqueous Cr (VI) reduction. J Hazard Mater 2012;223:1–12.
[26] Canizares P, et al. Electrodissolution of aluminum electrodes in electrocoagulation processes. Ind Eng Chem Res 2005;44(12):4178–85.
[27] Chaturvedi SI. Electrocoagulation: a novel waste water treatment method. Int J Mod Eng Res 2013;3(1):93–100.
[28] Jalil MER, Baschini M, Sapag K. Influence of pH and antibiotic solubility on the removal of ciprofloxacin from aqueous media using montmorillonite. Appl Clay Sci 2015;114:69–76.
[29] Li X, Yue P-L, Kutal C. Synthesis and photocatalytic oxidation properties of iron doped titanium dioxide nanosemiconductor particles. New J Chem 2003;27(8):1264–9.